Fabrication of a Boersch phase plate for phase contrast imaging in a transmission electron microscope

K. Schultheiß
Laboratorium für Elektronenmikroskopie, Universität Karlsruhe, D-76128 Karlsruhe, Germany

F. Pérez-Willard
Laboratorium für Elektronenmikroskopie, Universität Karlsruhe, D-76128 Karlsruhe, Germany and DFG Center for Functional Nanostructures, Universität Karlsruhe, D-76128 Karlsruhe, Germany

B. Barton
Department of Structural Biology, Max-Planck-Institute of Biophysics, D-60438 Frankfurt am Main, Germany

D. Gerthsen
Laboratorium für Elektronenmikroskopie, Universität Karlsruhe, D-76128 Karlsruhe, Germany

R. R. Schröder
Department of Structural Biology, Max-Planck-Institute of Biophysics, D-60438 Frankfurt am Main, Germany

(Received 19 December 2005; accepted 28 January 2006; published online 10 March 2006)

The Boersch phase plate for a transmission electron microscope (TEM) offers major advantages over other phase plate concepts. However, due to its miniature dimensions, it could not be constructed and implemented so far. We report the first successful fabrication of a Boersch phase plate, which was produced by a combination of electron-beam and focused ion-beam lithography on a freestanding silicon nitride membrane. The manufactured multilayer electrode structure was tested for its functionality as an electrostatic einzel lens in a TEM. First experiments show that it can be used as a phase shifting device, as proposed by Boersch, to optimize phase contrast transfer in transmission electron microscopy. © *2006 American Institute of Physics.*
[DOI: 10.1063/1.2179411]

I. INTRODUCTION

Since its development, the transmission electron microscope (TEM) has revolutionized the fields of solid state, materials and biological sciences. Its high spatial resolution, typically three orders of magnitude better than that of a conventional light microscope (LM), allows the study of objects on the scale of a few microns to 1 Å. In contrast to LMs, the resolution of the TEM is limited by the quality of electron lenses and coherence of the electron wave rather than by the wavelength of the utilized radiation (typically a few picometers in a TEM).

However, an additional, more stringent limitation to the accuracy of reconstructions by TEM is given by the nature of the sample under study itself. In particular, so-called weak-phase objects are difficult to image because they interact only weakly with the incident electron wave. Instead of modifying the amplitude of the interacting electron wave, weak-phase objects impose only small phase shifts on it, which produce very low observable contrast in a conventional bright-field TEM image. Ideally, an additional phase shift of $\pi/2$ between the unscattered and scattered electrons is required to obtain maximal phase contrast for a weak-phase object. Some examples of weak-phase objects are thin unstained biological specimens, consisting mainly of elements with low atomic numbers (C, O, N, H), thin amorphous films, magnetic domains, and samples containing small voids or gas bubbles.[1]

Usually, phase contrast in a TEM is generated by defocusing the objective lens deliberately.[2] Under such imaging conditions, defocus and the spherical aberration of the objective lens lead to a spatial frequency-dependent phase shift between the scattered and the unscattered part of the object exit wave. This phase shift then produces object contrast in the bright-field image. As a drawback, the object contrast is strongly dependent on the spatial frequency. In addition, low spatial frequencies $<1/5$ nm^{-1}, representing the outline of objects, e.g., single macromolecules, are imaged with almost negligible phase contrast. To overcome this problem the acquisition and subsequent digital processing of images recorded at different objective lens defoci (i.e., defocus series) is necessary.[3] In state-of-the-art aberration-corrected TEMs a second parameter, the spherical aberration, can be tuned in order to tailor the phase relationship between scattered and unscattered electrons.[4] However, this technique is only suited for maximizing high-resolution phase contrast for objects where high spatial frequencies distinctly above 1 nm^{-1} are relevant.

An electron-optical phase plate that produces a uniform relative phase shift between scattered and unscattered electrons for all spatial frequencies without defocusing the ob-

jective lens opens new vistas for high-resolution imaging of weak-phase objects. Zernike-type[5] phase plates, consisting of a thin amorphous carbon film with a small hole positioned in the center of the back focal plane of the objective lens, have successfully produced phase contrast in a TEM.[6] The scattered electrons undergo a phase shift within the mean inner Coulomb potential of the amorphous carbon film relative to the direct, unscattered beam, which is transmitted through the small hole in the film. A relative phase shift of $\pi/2$ is obtained if the thickness of the film is chosen appropriately. However, the carbon film is subject to rapid contamination and charging, and due to the loss of high-resolution signal as a result of incoherent scattering it is not routinely applied in high-resolution transmission electron microscopy.[6,7]

An alternative approach based on an electrostatic lens was proposed by Boersch in 1947.[8] In this case, the primary beam is phase shifted relative to the scattered electrons by the electrostatic potential inside a microstructured electrode, which is positioned in the back focal plane of the objective lens. The main advantage of this electrostatic phase shifting device over the Zernike-type carbon film phase plate is the use of the electrostatic field for obtaining a relative phase shift. Since scattered and unscattered electrons travel through vacuum, interactions of the electrons with matter that reduce the coherence of the electron wave are avoided. This makes electrostatic phase plates applicable for high-resolution imaging. Furthermore, by varying the voltage applied to the electrode, the relative phase shift can be tuned. Matsumoto and Tonomura proposed a technological realization for an electrostatic phase plate.[9] Although the advantages of the Boersch phase plate concept were always obvious, its fabrication had not been possible up to now.

Here, we report the first successful fabrication of a Boersch phase plate, which was produced by combining electron-beam and focused ion-beam lithography on a freestanding silicon nitride membrane. Our realization of the Boersch phase plate is based on the concepts proposed by Matsumoto and Tonomura[9] and Majorovits and Schröder.[7]

II. BASIC MATERIALS AND TOOLS FOR FABRICATION AND TEST OF THE PHASE PLATE

As the substrate material, commercially available 100 nm thick low-stress $Si_{3+x}N_{4-x}$ membranes were used.[10] The membranes are 200×200 μm in size and supported by a frame of 200 μm thick Si(100).

The phase plate electrode was defined on the $Si_{3+x}N_{4-x}$ membrane by standard electron-beam lithography and subsequent electron-beam evaporation of Au under high vacuum conditions. The shape of the phase plate was patterned in the membrane using the 30 kV Ga^+ focused ion beam (FIB) of a Zeiss EsB 1540 scanning electron microscope (SEM)/FIB dual-beam instrument equipped with an external Raith Elphy Plus pattern generator.

Finally, the phase plate was tested in a Zeiss SESAM II Cryo 200 keV energy filtering TEM (EFTEM). Its position in the back focal plane of the objective lens was controlled by means of a piezodriven Kleindiek MM3A micromanipulator.[11]

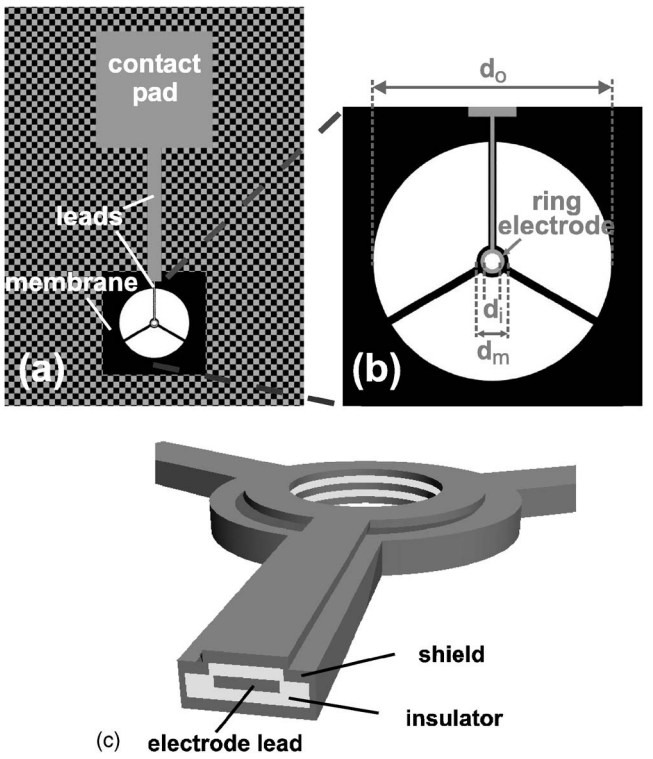

FIG. 1. (a) Schematic of a chip containing a Boersch phase plate, Au leads, and a macroscopic Au contact pad. (b) Zoom into the phase plate region on the freestanding membrane (in black). (c) Three-dimensional sketch of the central region of the phase plate.

III. FABRICATION PROCESS OF THE BOERSCH PHASE PLATE

Figure 1 schematically shows the design of the Boersch phase plate fabricated in this study. The phase plate has a circular aperture with an outer diameter d_o. In the center of the phase plate is a ring-shaped, multilayered structure with an outer and inner diameter d_m and d_i, respectively. This ring-shaped structure realizes an electrostatic lens, which acts as phase plate if low electric potentials are applied. The unscattered electrons are transmitted through the opening in the electrode, while the electrons scattered within the sample travel through the aperture between d_o and d_m. The ring-shaped structure is supported by three 3 μm wide bars which span the distance between the electrode ring and the outside edge of the phase plate. Neighboring bars form an angle of 120°, according to the suggestion of Majorovits and Schröder.[7] A noncentrosymmetric arrangement of the bars allows the restoration of the information encoded in the spatial frequencies blocked by the bars in the back focal plane by means of Friedel pair correction.[7]

The phase plate electrode is connected through a lead in one of the supporting bars to further leads outside the phase plate and finally to a macroscopic contact pad on the chip [see Fig. 1(a)]. The electrode, leads, and contact pad consist of Au. As shown in Fig. 1(c) the bars and the outside of the ring electrode are encased in an insulating material, Al_2O_3, and shielded by a Au cladding.

Application of an electric potential to the contact pad leads to an electric field, which originates only from the unshielded inner surface of the electrode ring, and thus is

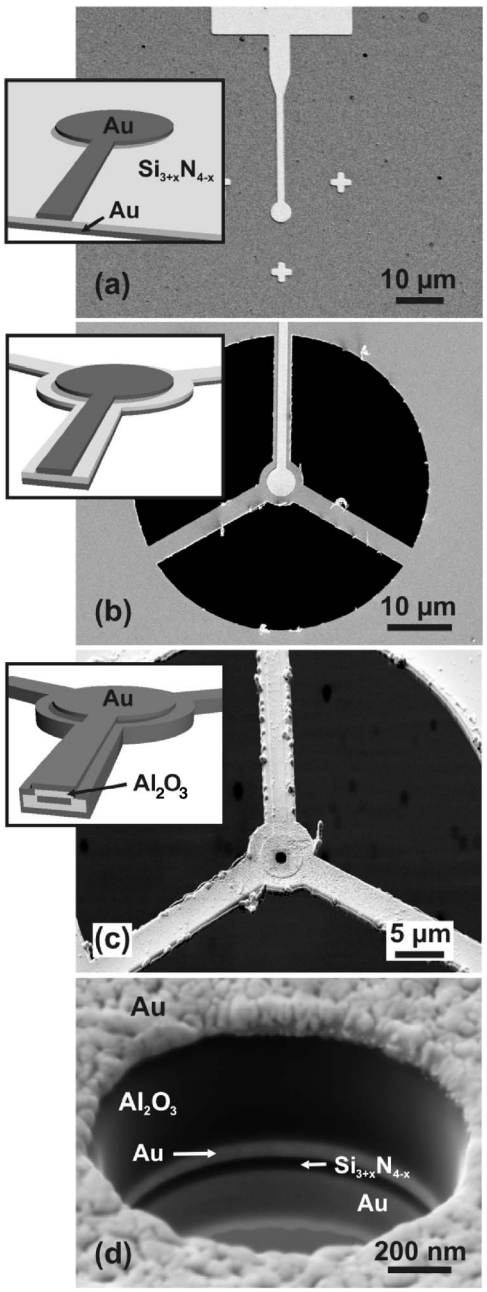

FIG. 2. SEM images illustrating the different steps of the fabrication process of the Boersch phase plate. (a) After electron-beam lithography, Au evaporation, and lift-off. (b) After the first FIB lithography step. [(c) and (d)] Finished phase plate. (d) Close-up view of the ring electrode hole.

strictly confined to the inside of the ring electrode. The electric field shifts the phase of the electrons passing through the ring relative to the phase of the scattered electrons which are transmitted through the aperture of the phase plate.[8] For low voltages the phase shift is expected to be uniform inside the ring (weak-lens approximation).[9]

The main steps in the fabrication process of the Boersch phase plate are illustrated in Fig. 2. A thin $Si_{3+x}N_{4-x}$ membrane was used as a substrate. The membrane itself constitutes one of the insulating layers needed to encapsulate the voltage carrying electrode (partially) and its leads. In the first step, the bottom side of the membrane is metallized with a 100 nm thick Au film. Next, the ring electrode, leads, and contact pad are fabricated on the top side of the membrane by conventional electron-beam lithography, subsequent Au evaporation, and lift-off. The result is shown in the SEM image in Fig. 2(a). The central electrode has a thickness of 50 nm.

To produce the silhouette of the phase plate—without the central opening of the ring electrode—the nitride membrane and the underlying Au layer were cut using FIB lithography. Typically, an ion current of ~500 pA was used. Cross-shaped markers, previously defined in the electron-beam lithography step [see Fig. 2(a)], allow the alignment of the FIB pattern and the given electrode structure with an accuracy of better than 100 nm. A SEM image of the resulting structure is shown in Fig. 2(b).

The layered structure of the phase plate is completed by electron-beam evaporation of a second insulating 250 nm layer of Al_2O_3 and a 100 nm layer of Au on the electrode side of the membrane. During this last Au deposition step the sample is rotated continuously around an axis, which is tilted by 45° to the main axis of the evaporation system in order to ensure that the Au shielding layer also covers the faces of the structure perpendicular to the membrane plane.

Finally, the central hole of the phase plate is milled in a second FIB patterning step. Figure 2 shows a SEM image of the central region of a finished phase plate [Fig. 2(c)] and a close-up view of the ring electrode hole [Fig. 2(d)], revealing the different layers of the phase plate.

IV. TESTING THE BOERSCH PHASE PLATE

Two of the fabricated Boersch phase plates were implemented and tested in a TEM. In this section results which were obtained for a phase plate with d_o=45 μm, d_m=7 μm, and d_i=1.6 μm are shown.

The phase plate chip was fixed in an aluminum holder and electrical connections were made to the contact pad and the shielding Au layer. The shielding layer was grounded. The aluminum holder was attached to a piezodriven manipulator, which allows the positioning of the phase plate in the back focal plane of the objective lens with a lateral accuracy of better than 10 nm. In diffraction mode the ring electrode can be centered around the central beam in the same way as a standard objective aperture. After alignment the phase plate is ready for operation.

A 1 nm amorphous W film on a 4 nm carbon support was used as a test sample. An amorphous film represents a spatial white noise containing all spatial frequencies and is therefore well suited for the analysis of spectral contrast transfer. To increase the visibility of higher spatial frequencies (larger scattering angles) in the spectrum, we used a heavy atom film such as tungsten.

Images were recorded at a primary magnification of 119.800× using a 1024×1024 pixel charge coupled device (CCD) camera. Power spectra were obtained by numerical Fourier transformation of the images. Figure 3 is composed of two power spectra based on images taken at constant objective lens defocus values, but at different phase plate electrode potentials of U_B=0 V (lower half) and U_B=1 V (upper half), respectively. The bright rings, so-called Thon rings,

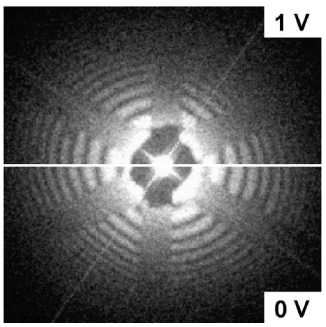

FIG. 3. Power spectra obtained from images of an amorphous W film observed in the TEM at a primary magnification of 119.500× for two different voltages, 0 V (lower half) and 1 V (upper half). For 1 V the Thon rings are uniformly shifted, indicating a uniform phase shift of $\varphi=\pi/2$ between scattered and unscattered electrons.

correspond to the maxima of the squared modulus of the contrast transfer function (CTF). The coherent phase CTF (PCTF) is given by Eq. (1). It is a function of the spatial frequency k, the electron wave length λ, the spherical aberration constant of the objective lens system C_s, and the objective lens defocus value Δf. A phase shift φ between scattered and unscattered electrons is additionally taken into account.

$$\mathrm{PCTF}(k) = 2\sin\left[\frac{\pi}{2}(C_s\lambda^3 k^4 - 2\Delta f k^2) + \varphi\right]. \quad (1)$$

The damping of the PCTF due to the partial temporal and spatial coherence of the electron beam is omitted in Eq. (1) for simplicity. The Thon ring pattern changes with increasing potential, reaching a phase shift of approximately $\pi/2$ at $U_B=1\pm0.05$ V. At this phase shift the sine term in the PCTF transforms into a cosine term. Figure 3 shows this situation where the maxima of the Thon ring patterns are almost complementary for $U_B=0$ V and $U_B=1$ V. It is important to note that this complementarity of the Thon rings is, within the experimental error, independent of the spatial frequency k. This was expected for the weak-lens approximation, where the deflection of the electrons by the electrostatic field is neglected.[9]

In the region close to the central beam, between d_i and d_m, the contrast transfer is completely blocked as a result of the solid electrode structure (see Fig. 3). In the future, the design of the phase plate will be optimized to reduce the width of the central electrode and its supporting bars, and so to minimize the loss of image information.

V. SUMMARY

We have developed a fabrication process suitable for the production of microscaled electrostatic lenses. In particular, this process was applied to realize the first Boersch phase plate for phase contrast imaging in a TEM. By applying a moderate electrostatic potential to the Boersch phase plate electrode, a phase shift of $\varphi=\pi/2$ of the unscattered electrons relative to the scattered electrons was achieved. The realization of Boersch's concept paves the way towards true phase contrast imaging in TEM.

ACKNOWLEDGMENTS

The authors thank T. Kuhn (Institute for Applied Physics, University of Karlsruhe, Germany) for the operation of the electron-beam evaporation system. Furthermore, the authors thank Drs. R. Danev and K. Nagtavama (Okazaki National Research Institutes, Okazaki, Japan) for the introduction to phase plate microscopy and Dr. K. C. Holmes (Max-Planck-Institute for Medical Research, Heidelberg, Germany) for continuous support and stimulating discussions. This work was supported by the DFG through the Center for Functional Nanostructures (CFN). It has been further supported by a grant from the Ministry of Science, Research and the Arts of BadenWürttemberg (Az: 7713.14-300).

[1] D. B. Williams and C. B. Carter, *Transmission Electron Microscopy* (Plenum, New York, 1996).
[2] O. Scherzer, J. Appl. Phys. **20**, 20 (1949).
[3] P. A. Penczek, J. Zhu, R. R. Schröder, and J. Frank, Scanning Microsc. Suppl. **11**, 145 (1997).
[4] M. Lentzen, Ultramicroscopy **99**, 211 (2004).
[5] F. Zernike, Physica (Amsterdam) **9**, 686 (1942).
[6] R. Danev and K. Nagayama, Ultramicroscopy **88**, 243 (2001).
[7] E. Majorovits and R. R. Schröder, Proceedings of the 15th ICEM, Durban, South Africa, 2002 (unpublished); E. Majorovits, Ph.D. thesis, Ruprecht-Karls-University, Heidelberg, 2002.
[8] H. Boersch, Z. Naturforsch. A **2A**, 615 (1947).
[9] T. Matsumoto and A. Tonomura, Ultramicroscopy **63**, 5 (1996).
[10] Silson Ltd., UK.
[11] Kleindiek Nanotechnik GmbH, Germany.